PERGAMON

Journal of Structural Geology 24 (2002) 485–499

JOURNAL OF STRUCTURAL GEOLOGY

www.elsevier.com/locate/jstrugeo

The influence of strain localisation on the rotation behaviour of rigid objects in experimental shear zones

Saskia M. ten Grotenhuis*, Cees W. Passchier, Paul D. Bons

Tectonophysics, University of Mainz, Becherweg 21, 55099 Mainz, Germany

Received 17 November 2000; revised 1 June 2001; accepted 13 June 2001

Abstract

Mica fish and tourmaline fish from natural mylonites were analysed in thin section to determine their orientation distribution. They are oriented with their long axes tilted with respect to the mylonitic foliation, and fish with a small aspect ratio exhibit a slightly larger angle than fish with a large aspect ratio. This orientation seems to be a stable orientation for the mica and tourmaline fish. Analogue experiments with two rheologically different matrix materials were performed to explain the data. One material was PDMS, a linear viscous polymer. The other was tapioca pearls, a granular material with low cohesion and Mohr–Coulomb type behaviour. In contrast to a fairly homogeneous strain distribution in PDMS, distinct small-scale shear bands developed in tapioca pearls during deformation. Experiments modelled different vorticity numbers and parallelogram-shaped rigid objects with different aspect ratios were used. Rotation rates of objects in a viscous matrix are very similar to analytical solutions for ellipses in viscous flow, but stable orientations differ from data of natural examples. In all experiments with a Mohr–Coulomb matrix elongated objects had a stable orientation due to small-scale strain localisation. We therefore suggest that small-scale strain localisation (≤mm) that might be hidden by ongoing deformation and recrystallisation processes, is an important characteristic of the rheology of mylonites.

Keywords: Strain localisation; Rotation behaviour; Analogue modelling; Rheology

1. Introduction

Mylonitic rocks usually contain porphyroclasts that can develop into shear sense indicators such as sigma and delta clasts, or lenticular structures such as mica fish (e.g. White et al., 1980; Simpson and Schmid, 1983; Lister and Snoke, 1984; Passchier and Simpson, 1986; Hanmer and Passchier, 1991; Passchier and Trouw, 1996). The understanding of these structures is essential for the correct interpretation of flow kinematics in mylonites.

To gain a better understanding of the behaviour of porphyroclasts in mylonites, analytical and experimental studies have investigated the behaviour of single or multiple objects or inclusions in a homogeneous viscous matrix. The rheology of a deforming mylonite is usually described as non-linear viscous, with a power-law relationship between strain rate and stress (Kirby and Kronenberg, 1987). Although the stress exponent, n, which defines the sensitivity of strain rate to stress is usually assumed to be 1–3 in mylonites, most modelling studies on porphyroclast behaviour assumed linear (Newtonian) viscous behaviour with $n = 1$. Jeffery (1922) showed that the rotation rate of an elliptical object in a linear viscous matrix in simple shear is a function of the strain rate, and of the aspect ratio and orientation of the object. Solutions for pure shear flow (Gay, 1968) and combinations of pure and simple shear, general flow (Ghosh and Ramberg, 1976), have also been proposed. This early work has been extended to the motion of rigid objects in non-Newtonian fluids by Ferguson (1979) and to triaxial elliptical objects by Hinch and Leal (1979), Freeman (1985), Passchier (1987) and Jezek et al. (1994) for example. According to the equations for rigid elliptical objects in a Newtonian viscous fluid, all objects, except lines and planes, rotate continuously in simple shear. Elongated or flat objects have a pulsating rotation rate under these conditions. In plane strain general flow with a kinematic vorticity number (W_k, Means et al., 1980) between zero and one, elliptical objects rotate towards a stable orientation, if their aspect ratio exceeds a critical value (R_{crit}). R_{crit} is a function of the kinematic vorticity number (Ghosh and Ramberg, 1976; Passchier, 1987):

$$R_{crit} = \sqrt{\frac{1 + W_k}{1 - W_k}}$$

* Corresponding author. Present address: HPT-laboratory, Faculty of Earth Sciences, P.O. Box 80021, 3508 TA Utrecht, The Netherlands. Tel.: +31-30-2531177.

E-mail address: saskiatg@geo.uu.nl (S.M. ten Grotenhuis).

0191-8141/02/$ - see front matter
PII: S0191-8141(01)00072-4

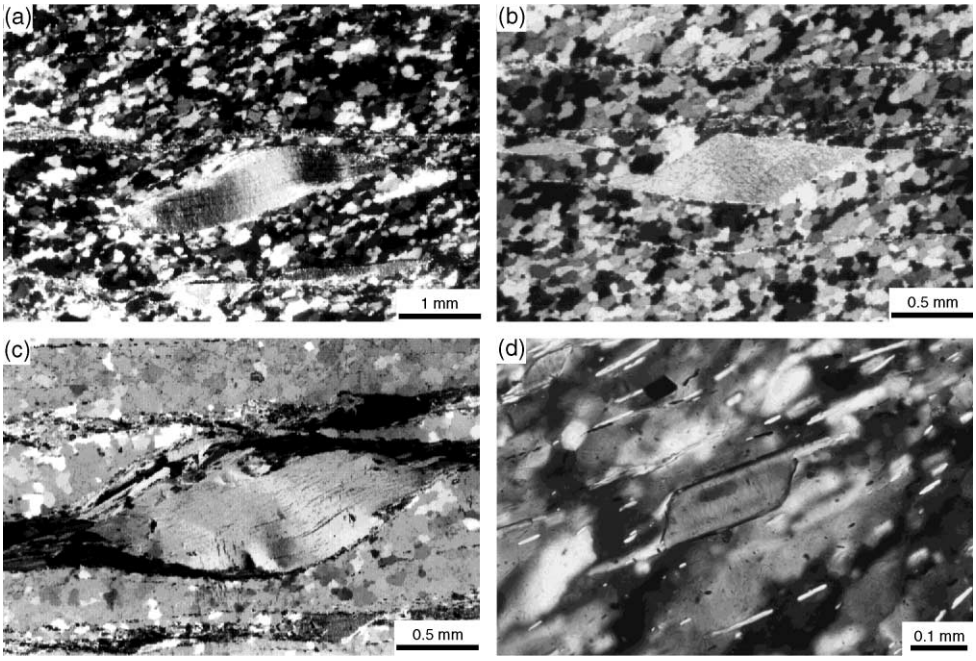

Fig. 1. Photomicrographs of mica and tourmaline fish in thin sections parallel to the stretching lineation and perpendicular to the foliation. The shear sense is dextral in all pictures. (A) Lenticular-shaped muscovite fish from Conceição do Rio Verde, Brazil. (B) Parallelogram-shaped muscovite fish from Conceição do Rio Verde, Brazil. (C) Lenticular biotite fish from the Santa Rosa mylonite zone, California, USA. (D) Parallelogram-shaped tourmaline fish from Lambari, Brazil.

Objects with a lower aspect ratio rotate continuously, but with a pulsating rotation rate. In simple shear ($R_{crit} = \infty$) there are no stable orientations except for lines and planes. In pure shear ($R_{crit} = 1$) all objects rotate towards a stable position, and spheres are stationary.

Several aspects of the deformation of porphyroclast systems have been studied in analogue experiments and numerical modelling. For the behaviour of rigid objects in a ductile matrix different materials have been used as an analogue for the matrix, such as silicon putty (e.g. Ghosh and Ramberg, 1976; Ildefonse et al., 1992a; Arbaret et al., 2001), honey with titanium oxide (Fernandez et al., 1983; Ildefonse et al., 1992b), paraffin wax (Ildefonse and Mancktelow, 1993), octachloropropane (OCP), polyacrylamide (pAA) solution, and glycerine (ten Brink, 1996). These experiments modelled either simple or pure shear flow and rigid objects were rectangular or of monoclinic shape. In single particle experiments for most matrix materials, Newtonian and non-Newtonian, the embedded objects behave as predicted by the analytical solutions mentioned above for elliptical objects with a similar aspect ratio. In the case of a non-coherent boundary (Ildefonse and Mancktelow, 1993) and for experiments with an anisotropic non-Newtonian viscous matrix material (OCP and pAA solution, ten Brink, 1996) the rotation rate of the rigid objects in simple shear is slower as predicted by analytical solutions (Jeffery, 1922). These results indicate that certain properties of the matrix can have a major effect on the behaviour of porphyroclasts. Multi-particle experiments (Ildefonse et al., 1992a,b; Ildefonse and Mancktelow, 1993; Tikoff and Teysier, 1994; Arbaret et al., 1997) show that interaction of the objects results in a preferred orientation of the objects. Some objects in these experiments rotate backwards, i.e. clockwise in sinistral simple shear (Ildefonse and Mancktelow, 1993). Numerical models mainly concentrate on the flow perturbation around a rigid object (Bons et al., 1997; Pennacchioni et al., 2000). The analytical solutions by Jeffery (1922) and Ghosh and Ramberg (1976) predict that after large strains most objects of an initially randomly distributed population of elongated objects are orientated close to the orientation of minimum rotation rate. Vorticity analyses, based on the orientation distribution of objects in natural shear zones were done by several authors (e.g. Passchier, 1987; Jezek et al., 1994; Masuda et al., 1995). Masuda et al. (1995) made distribution plots of aspect ratio versus orientation for initially randomly distributed objects in plane strain flow after different amounts of finite strain, to predict both the vorticity number of flow and finite strain in mylonites.

In this study attention is paid to the behaviour of objects with a parallelogram shape in simple shear and combinations of pure and simple shear. In natural shear zones objects with a parallelogram or lenticular shape are common as so-called mica fish, usually composed of muscovite or biotite (Eisbacher, 1970; Fig. 1). Similar structures can also be formed by other minerals, such as garnet (Azor et al., 1997) and tourmaline (Fig. 1). From observations on natural mica fish by Eisbacher (1970) and Lister and Snoke (1984) it is known that mica fish usually have a similar orientation independent of strain intensity, with their long axis inclined

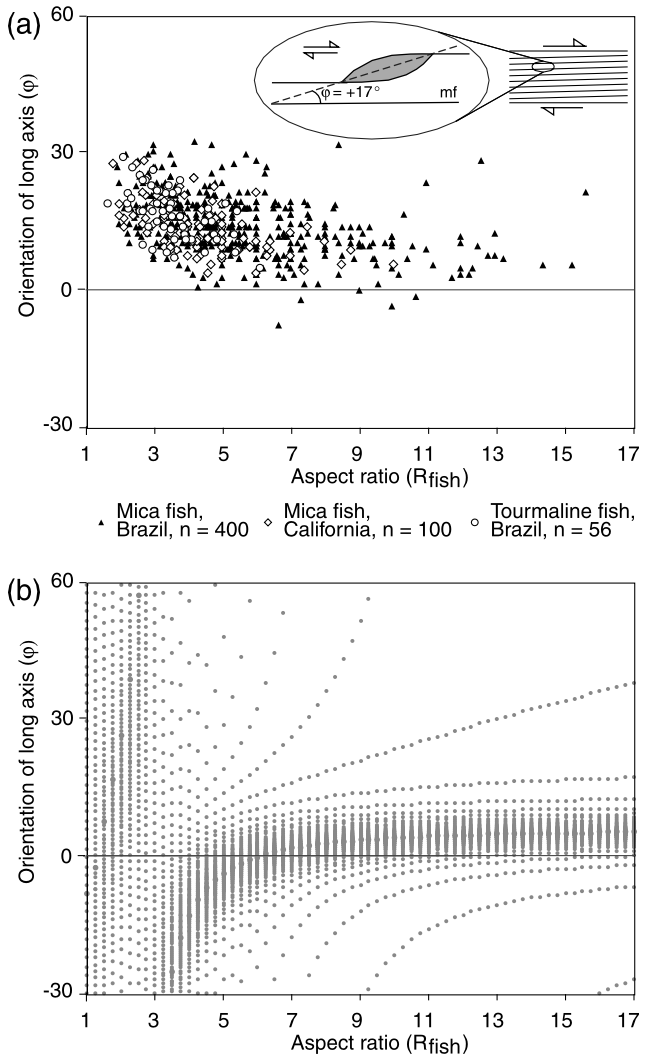

Fig. 2. (a) Plot of the orientation of long axis with respect to aspect ratio (long axis/short axis) of mica and tourmaline fish. Inset shows definition of φ with respect to the foliation observed in the field (mf = mylonitic foliation) and the sign convention used throughout this paper. (b) The distribution pattern of initially homogeneously distributed ellipses for simple shear after a shear strain of $\gamma = 10$, according to the solutions of Jeffery (1922) (after Masuda et al. (1995), changed to conform to the sign convention used in this paper).

at about 10–20° with respect to the flow plane. This suggests that they rotated towards a stable orientation. This orientation is different from the stable or slow rotation rate orientation of elongate rigid objects predicted by theory (Jeffery, 1922) and observed in experiments with rigid objects in a viscous matrix (e.g. Ghosh and Ramberg, 1976). We tried to investigate how the orientation of these structures can be explained and what this tells us about the flow kinematics and rheology in ductile shear zones. The shape and orientations of mica and tourmaline fish from three different localities are described and the observed geometries and orientations were used as a basis to perform a number of analogue experiments.

2. Measurements of natural samples

Two sets of mica fish and one set of tourmaline fish were analysed in thin sections to determine their orientation distribution. The first set, isolated muscovite fish within pure quartzite, comes from a shear zone near Conceição do Rio Verde, Southern Minas Gerais State, Brazil (Trouw et al., 1983). The quartzites belong to the lower unit of the Neoproterozoic Andrelândia Depositional Sequence (Paciullo et al., 1993; Ribeiro et al., 1995). The outcrop (45°06′W, 21°56′S) is located in an ENE-trending, subvertical greenschist facies dextral shear zone, about 500 m thick. In 3D the mica fish have a flake or disc shape. In the plane parallel to the stretching lineation and perpendicular to the foliation the mica fish are elongated and have a parallelogram or lenticular shape (Fig. 1a and b). The aspect ratio (R_{fish} = longest axis/shortest axis) of the fish in this plane is between 2 and 16, with an average of 5.7 (Fig. 2a). Trails of small mica particles, apparently separated from the mica fish by a process of dynamic recrystallisation or cataclasis, extend from the tips of the mica fish into the matrix. These 10–100-μm-wide trails define a microscopic foliation (Simpson and Schmid, 1983; Passchier and Trouw, 1996). This foliation is referred to as the mylonitic foliation, and is parallel to the macroscopic foliation in the shear zone. The matrix surrounding the mica fish consists of fine-grained quartz with a crystallographic preferred orientation (CPO) and a shape preferred orientation (Means, 1981; Lister and Snoke, 1984), which makes an average angle of 34° with the mylonitic foliation. The mica fish are inclined to the mylonitic foliation in the same direction as the oblique foliation. The angle (φ) between the long axes of 400 measured mica fish and the mylonitic foliation has a median value of 13° (Fig. 2a).

The second set of samples comes from the Santa Rosa mylonite zone, Palm Canyon, California. The mica fish are developed in mylonitised granodiorites, which are present in a 700–900-m-thick sequence of mylonites in Palm Canyon (Wenk and Pannetier, 1990). These mylonites are related to a thrust system and deformation occurred at middle amphibolite facies conditions (Simpson, 1984; Wenk and Pannetier, 1990; Goodwin and Wenk, 1995). The matrix is composed of quartz with a CPO. The mica fish from this location are both muscovite and biotite fish (Fig 1c). One hundred (31 muscovite and 69 biotite) mica fish aspect ratios were measured, ranging from $R_{\text{fish}} = 2$–10, with an average of 4.3 (Fig. 2a). The mica fish from this shear zone are also oriented with their long axis inclined with respect to the mylonitic foliation. The median value of φ for this shear zone is 12° for the biotite fish and 15° for the muscovite fish.

The third set of samples contains tourmaline fish (Fig. 1d) and comes from a shear zone near Lambari, Southern Minas Gerais State, Brazil (Trouw et al., 1983) in the Andrelândia Depositional Sequence (Paciullo et al., 1993; Ribeiro et al., 1995). Deformation in these samples occurred under middle

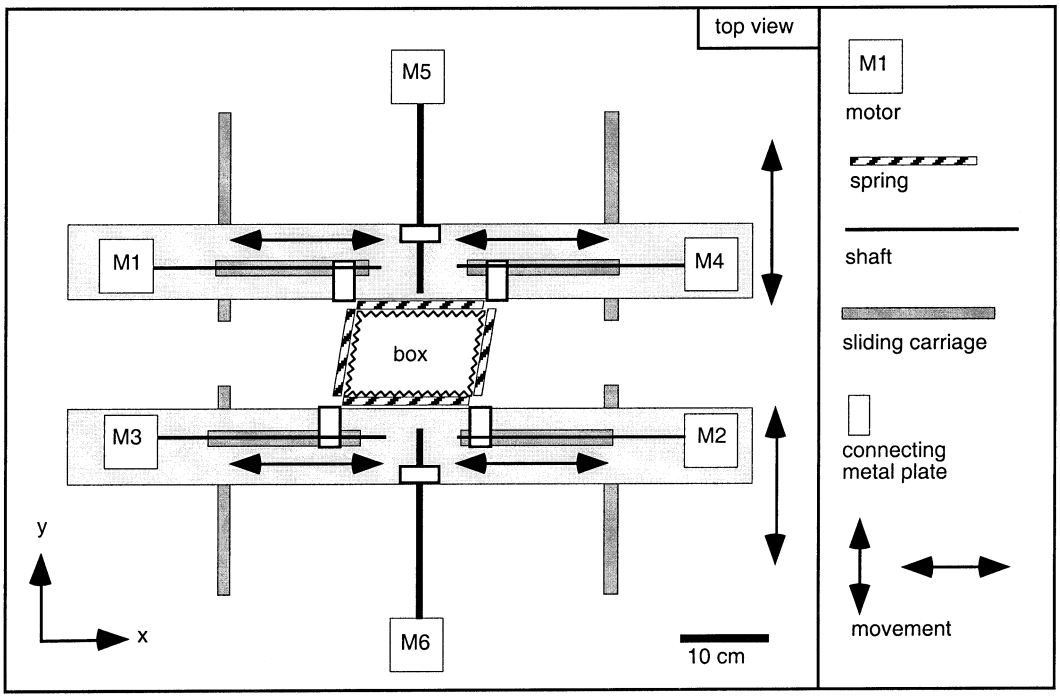

Fig. 3. Schematic drawing of the deformation apparatus, seen from the top. The sides of the box can be independently moved by the six motors to create any type of bulk monoclinic flow.

amphibolite facies conditions. The matrix consists of fine-grained quartz with a CPO. In contrast, with the smoother mica fish the tourmaline fish have an angular parallelogram shape with straight sides and an angle of about 50–55° between the sides (Fig. 1d). Their long side is usually parallel to the mylonitic foliation. The aspect ratio $R_{fish} = 1.5–6$. The angle φ has a median value of 17° for the tourmaline fish (Fig. 2a).

The data from each location show similar trends; fish with a small aspect ratio have on average a relatively high angle with the mylonitic foliation. The overlap between the data of the three sets of samples indicates that the orientation is independent of the strain intensity in the shear zone. Apparently this orientation is a stable orientation, depending only on the aspect ratio of the object. The distribution pattern of the longest axes of initially homogeneously distributed ellipses for simple shear after a shear strain of $\gamma = 10$ (Masuda et al., 1995) is plotted in Fig. 2b for comparison with analytical work on elongated objects. A shear strain of $\gamma = 10$ is chosen, since the monoclinic fabric and the straight foliation and lineation on outcrop scale suggest high strain and while it also fits reasonably well with the data for mica fish with an aspect ratio $R_{fish} > 8$. The distribution of objects with a smaller aspect ratio, however, does not resemble the distribution pattern of the natural mica and tourmaline fish. None of the other distribution plots of aspect ratio with respect to orientation of rigid ellipsoids of Masuda et al. (1995) shows a resemblance to the pattern observed in Fig. 2a. Lister and Snoke (1984) suggested that inhomogeneous flow of the matrix might play a role in mylonites containing mica fish. Observation of boudinaged mica fish, linked by fine-grained mica trails could be taken as evidence that part of the deformation is accommodated in narrow zones in the investigated mylonites, as in the case of *S–C* mylonites (Berthé et al., 1979; Lister and Snoke, 1984). However, the mylonites with mica fish studied by us show no decrease in grain size, change in CPO or other signs of enhanced strain towards the trails of mica grains. The trails of mica particles are mostly parallel without the anastomosing geometry seen in many ductile shear zones with flow partitioning. Another possibility could be that these trails represent the long axis of the finite strain ellipsoid. Clearly, the orientation of the mica fish is a crucial feature for the correct interpretation of this microstructure. We therefore carried out two sets of experiments with contrasting rheological matrix properties to compare with the observed object orientations: one with a homogeneous viscous material and one with extreme flow localisation.

3. Experimental set-up

3.1. The apparatus

The experiments were performed with a deformation apparatus that can model deformation in general flow regimes. The apparatus (Piazolo et al., 2001) consists of a four-sided deformation box with walls constructed from 1 cm wide, 12 cm high Plexiglas segments, which are

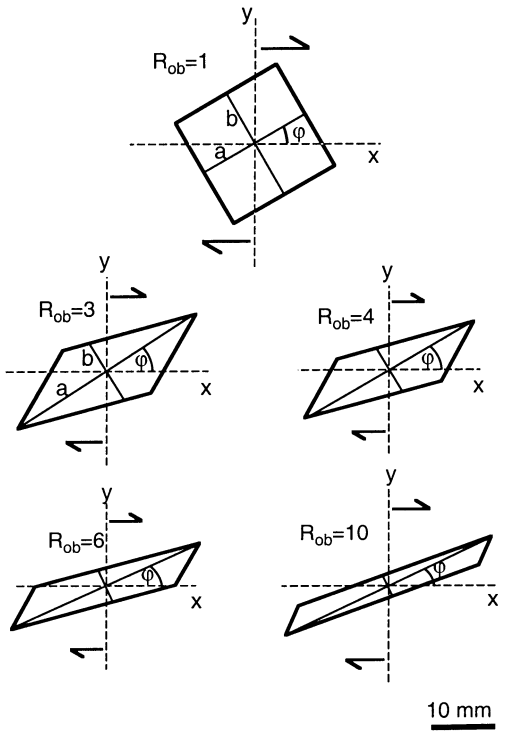

Fig. 4. Schematic drawing of the rigid objects used in the experiments, with angles used to describe their orientation (φ).

connected with flexible plastic (Fig. 3). The segments are connected at the outside to two metal springs. This construction ensures homogeneous contraction and extension of the walls. Two opposite sides of the deformation box, each consisting of 30 segments, are always parallel to the *x*-direction of the *x, y, z*-reference frame of the apparatus (Fig. 3). The two other sides, made of 20 segments each, can rotate about the *z*-axis. A 0.35-mm-thick elastic latex sheet forms the bottom of the deformation box. This construction results in a deformation box that slides with low friction on the base plate and which is open at the top. The contraction or extension of the flexible sides of the deformation box is controlled by six stepping motors. This set-up allows all types of monoclinic flow to be modelled. Boundary effects extend 10–15 mm into the matrix from the walls (Piazolo et al., 2001). Velocity of the motors is controlled by the computer program LabView®.

Table 1
Dimensions of the objects

Particle name	*a* (mm)	*b* (mm)	*c* (mm)	Angle[a] (°)
3	22.5	7.5	24.0	45
4	22.0	5.5	33.0	45
6	27.5	4.5	21.5	45
10	35.0	3.5	21.5	45
1rect	20.5	20.5	41.0	90

[a] Sharp angle between the sides of the object.

3.2. Experimental procedure

Experiments were carried out in dextral plane strain non-coaxial progressive deformation, also known as sub-simple shear (Simpson and De Paor, 1993) or stretching shear zone geometry (Passchier, 1998). The kinematic vorticity number values of deformation modelled in the experiments were 1 (simple shear), 0.95, 0.8 and 0.6. Two different analogue matrix materials were used. (1) PDMS (polydimethylsiloxane, trade name SGM 36, produced by Dow Corning, UK), a transparent viscoelastic polymer with a density of 0.97 g/cm^3 (Weijermars, 1986). At the strain rates used in this study, PDMS exhibits Newtonian viscous behaviour with a viscosity of 5.0×10^4 Pa s at room temperature. (2) As an analogue with extreme flow localisation we searched for a material with semi-brittle behaviour and low cohesion. We settled for densely packed tapioca pearls, approximately equidimensional spheres with a cross-section of 2.0 ± 0.4 mm. The tapioca pearls show Mohr–Coulomb type behaviour similar to sand, but with a low cohesion that is suitable for the deformation apparatus. The coefficient of internal friction, μ, and cohesion, C_0, for failure in tapioca pearls are: $\mu = 0.74 \pm 0.05$ and $C_0 = 39 \pm 44$ Pa (Appendix A).

Rigid blocks of India rubber with a density of 1.46 g/cm^3 are used as analogues for the mica and tourmaline fish. The objects are always placed with their flat top side parallel to the base plane (*xy*-plane) of the apparatus. In the *xy*-plane the objects had two principal shapes, parallelogram shape and square (Fig. 4). Parallelogram shapes in the *xy*-plane were used as analogues to natural mica and tourmaline fish. The angle between the sides was 45° and aspect ratios (R_{ob}) were 3, 4, 6, and 10 (Fig. 4). The square object ($R_{ob} = 1$) was used for reference. The major and minor axes of the object in the *xy*-plane are referred to as the *a*-axis and *b*-axis (Fig. 4; Table 1). The *c*-axis of the object is always parallel to the *z*-axis of the apparatus. Only the ratio between the *a*- and *b*-axes is important for the behaviour of the object in this orientation according to the analytical equations of Jeffery (1922). The orientation of the *a*-axis of the objects (φ) was measured with respect to the *x*-direction, i.e. the shear plane of the apparatus. Objects were placed with their long axis perpendicular to the *x*-direction ($\varphi = 90°$) or in the *x*-direction ($\varphi = 0°$) at the start of the first run of each experiment. Table 2 gives an overview of the performed experiments with the used strain rates.

The finite strain that can be achieved in the apparatus is limited to $\gamma = 3$ for $W_k = 1$ and to a stretch of 150% along the *x*-axis of the apparatus for $W_k < 1$. Higher strains were achieved by running series of experiments (cf. Passchier and Simpson, 1986). The precise orientation of the object was photographed and measured after each experimental run. After returning the box to the starting position the object was placed in the recorded final orientation and another experimental run under the same conditions as the previous run was carried out. This technique is particularly useful

Table 2
List of performed experiments: TP = tapioca pearls

Vorticity number (W_k)	Matrix material	R_{ob} of studied objects, starting orientation $\varphi_0 = 90°$	R_{ob} of studied objects, starting orientation $\varphi_0 = 0°$	Strain rate ($W_k = 1$) or stretching rate ($W_k < 1$) (s^{-1})
1	PDMS	1rect, 3, 4, 6		$2\ 10^{-3}$
1	TP	1rect, 3, 4, 6, 10	4	$2\ 10^{-3}$
0.95	TP	3, 4, 6, 10	3, 6	$3.3\ 10^{-4}$
0.8	PDMS	3, 4, 6		$3.3\ 10^{-4}$
0.8	TP	3, 4, 6, 10	10	$3.3\ 10^{-4}$
0.6	TP	3, 4, 6, 10	4	$3.3\ 10^{-4}$

when studying one or a few rigid objects. For the experiments with tapioca pearls there was an overlap of at least 10% between the runs, to control if the rotation rate of the object was the same at the end of a run and the beginning of the next run. This was the case for all experiments, because the strain 'memory' of the tapioca pearl aggregate is very low. Experiments presented here were run until the object stopped rotating for a strain of at least $\gamma = 0.5$ or stretch along the x-axis of 105%, or if the object had rotated a full 180°. Images of the sample were taken with a digital camera with a resolution of 800×600 pixels. The orientation of the objects was measured the same way as the natural mica fish and the accuracy of the measured orientation is 0.5°. We present the orientation of the object (φ) as a function of the simple shear component of deformation (γ) rather than strain ratio R_f. This is done for two reasons: (a) the equations given by Ghosh and Ramberg (1976) give the orientation as a function of the simple shear component of deformation, and (b) this component increases in a linear way with time at constant vorticity number and strain rate, unlike the strain ratio (R_f).

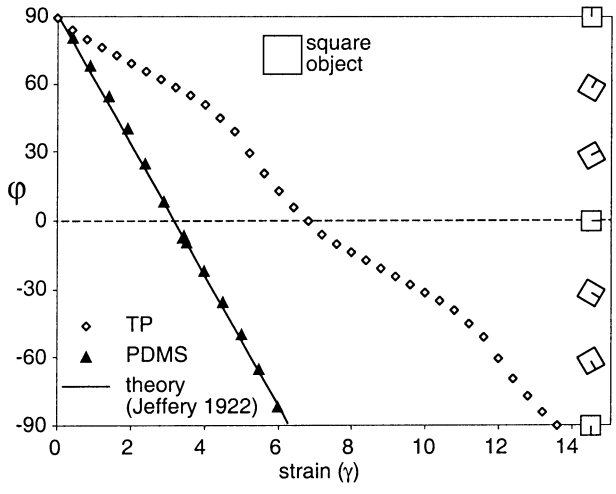

Fig. 5. Object orientation (φ) versus strain for experiments with a square object with two different matrix materials. Solid thick line indicates expected orientation of the object according to analytical solutions of Jeffery (1922) for a circular object.

4. Experimental results

4.1. Objects orientation

The results for simple shear experiments with the square object ($R_{ob} = 1$) in PDMS and tapioca pearls matrices are shown in Fig. 5. The rotation rate of the object in PDMS is constant and similar to the rate predicted by theoretical solutions. In tapioca pearls the object is also continuously rotating, but at a lower rate, as in PDMS, and the rotation rate is not constant. The minimum and maximum rotation rates in tapioca pearls are reached when the object has an orientation of $\varphi = 65$–75 and 20–30°, respectively.

Fig. 6 shows the results of the experiments with elongate objects in PDMS for $W_k = 1$ and 0.8. In simple shear ($W_k = 1$) the rotation rate of the objects has a minimum and maximum when their long axis is orientated at $\varphi = 0$ and 90°, respectively, like in analytical solutions for elliptical objects (Jeffery, 1922). For objects with $R_{ob} = 3$ and 4 the curves are very similar to the analytical solution for ellipsoids with the same aspect ratio. For $R_{ob} = 6$, the analytical solution for an ellipse with a slightly smaller aspect ratio ($R_{ob} = 5.6$) fits better. In experiments with a vorticity number of 0.8, all objects reach a semi-stable orientation with a small negative φ-value (Table 3) as predicted by Ghosh and Ramberg (1976). Objects with $R_{ob} = 3$, 4, and 6 closely follow the rotation rates predicted by analytical solutions for $W_k = 0.8$.

Fig. 7 shows the results for experiments with elongate objects in a matrix of tapioca pearls for $W_k = 1$ (simple shear). From a starting orientation of $\varphi_0 = 90°$, all objects rotated clockwise in the dextral shear. Their rotation rate decreased with increasing finite strain to reach a stable orientation, which is different for each aspect ratio. In all cases this orientation is at a positive angle ($\varphi > 0$). These results are completely different from the analytical solutions given by Jeffery (1922) and Ghosh and Ramberg (1976) for an elliptical object in simple shear. One experiment starting with $\varphi_0 = 0°$ was performed for the monoclinic object with $R_{ob} = 4$ to check if this angle corresponds to a stable or a semi-stable orientation. In this case the object started to rotate *counterclockwise* and reached the same orientation as for the experiment with $\varphi_0 = 90°$. This indicates that

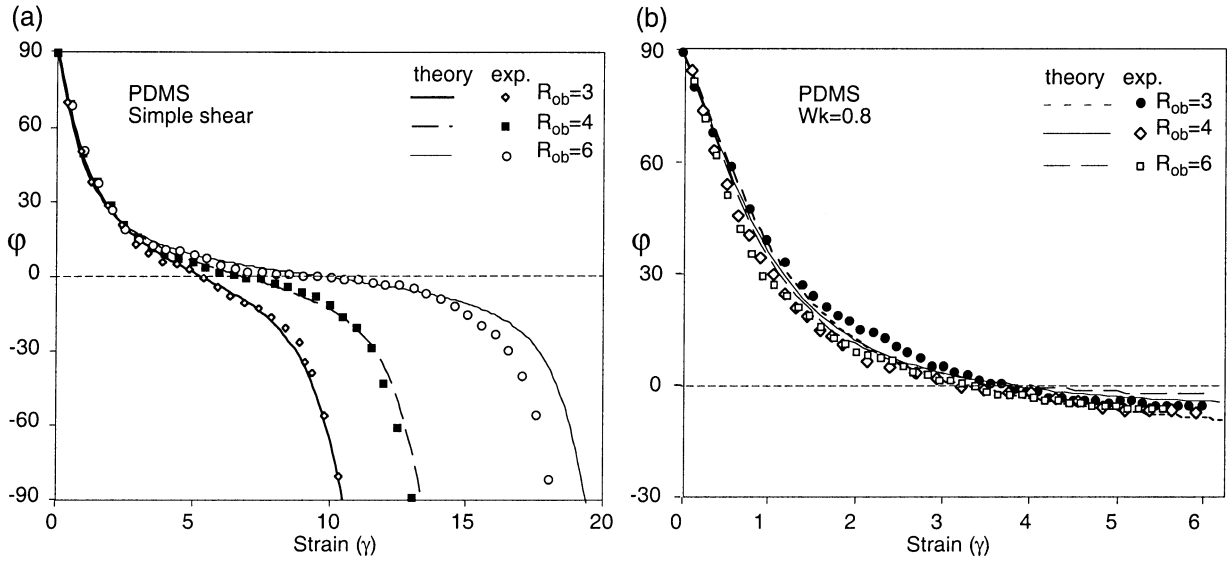

Fig. 6. Object orientation (φ) versus strain for different object aspect ratios with PDMS as a matrix material. Analytical solutions according to Jeffery (1922) are given as solid or dashed lines. (a) Simple shear $W_k = 1$. (b) $W_k = 0.8$.

the small positive angle is indeed a stable orientation for the object. The stable orientation (φ_{stable}) is a function of the aspect ratio; it decreases with increasing aspect ratio. This corresponds well with the observations for mineral-fish in natural shear zones (Fig. 2a).

The results for the experiments with tapioca pearls as matrix material with vorticity numbers 0.95, 0.8 and 0.6 are given in Fig. 8. The objects in these experiments show the same trend as in experiments with $W_k = 1$. For $\varphi_0 = 90°$ all objects start to rotate clockwise, towards a stable orientation (Table 3). Experiments with $\varphi_0 = 0°$ gave the same stable position as the experiments with $\varphi_0 = 90°$ for the same objects under the same conditions. The stable orientation (φ_{stable}) as a function of aspect ratio of the object (R_{ob}) for all experiments is plotted in Fig. 9. For experiments with a tapioca pearls matrix the maximum value for φ_{stable} is observed for the object with $R_{ob} = 3$ in simple shear. Additionally it is shown that for all objects the lowest angle is observed for the experiments with $W_k = 0.95$.

4.2. Analyses of strain distribution

Strain distribution during a strain increment within the sample was determined using pattern matching software 'PatMatch' (Bons and Jessell, 1995). With this program the distribution of deformation during each strain increment can be determined. Carbon powder was used as marker particles in the experiments with PDMS. In the experiments with tapioca pearls, individual grains could be traced. Both materials were first investigated in the absence of a rigid object. In deforming PDMS, strain is distributed relatively homogeneously throughout the material (Fig. 10a; Piazolo et al., 2001). In a matrix of tapioca pearls the strain is partly concentrated in small fault zones or shear bands for $W_k = 1$ (Fig. 10b), where the shear bands are approximately parallel to the *xz*-plane of the apparatus. The regions between these zones show little deformation. For $W_k = 0.8$ strain is distributed relatively homogenously (Fig. 10b). Some shear bands are developed close to the sides of the deformation box, which accommodate only a minor part of the deformation. Analysis of the experiments with PDMS with a central object (Fig. 11) shows that the finite strain is distributed very homogeneously during the analysed time interval. Analysis of the experiments with tapioca pearls with a central object in its stable position show that for all vorticity numbers micro faults or shear bands developed in

Table 3
Stable orientations (φ) of the particles; –object does not have a stable orientation under these conditions

Object (R_{ob})	PDMS		Tapioca pearls			
	$W_k = 1$	$W_k = 0.8$	$W_k = 1$	$W_k = 0.95$	$W_k = 0.8$	$W_k = 0.6$
3	–	− 5.6	24.4	2.9	10.7	10.8
4	–	− 4.4	16.7	8.8	13.5	10.8
6	–	− 4.4	14.4	4.9	14.4	12.4
10			11.8	0.4	8.7	12.1
1rect	–		–			

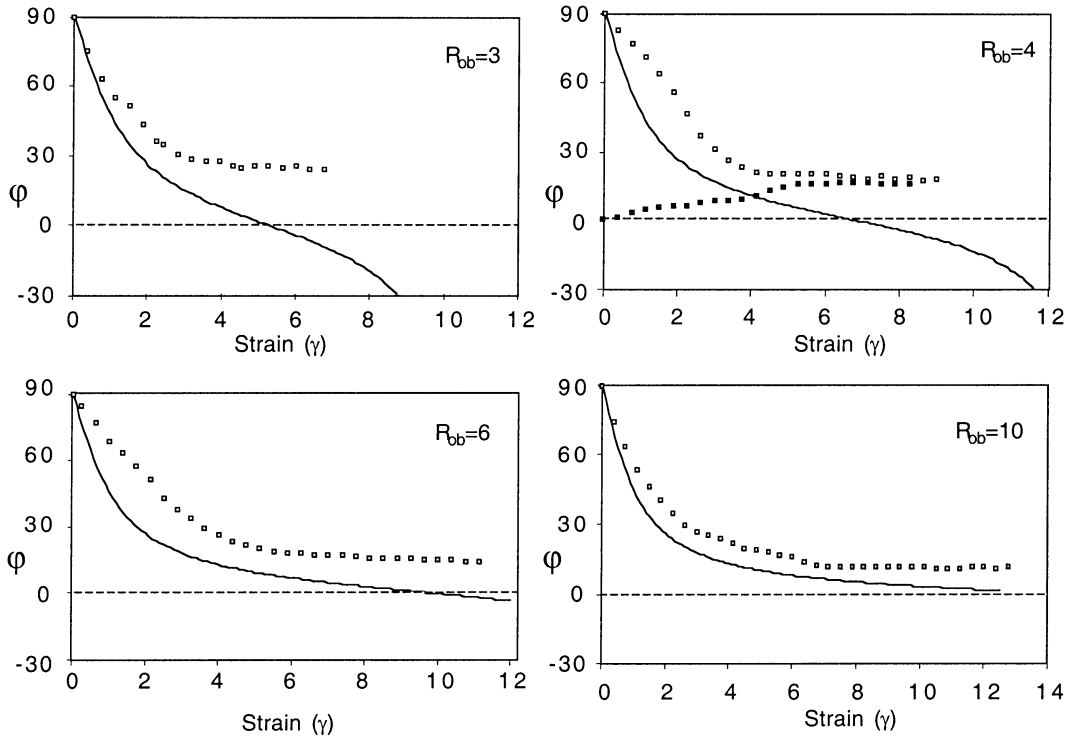

Fig. 7. Object orientation (φ) versus strain for experiments with tapioca pearls matrix with four different objects. All experiments model simple shear deformation. Initial orientation for the objects is $\varphi_0 = 90°$ for all objects and $\varphi_0 = 0°$ for an additional experiment with the object with $R_{ob} = 4$. Solid lines are analytical solutions according to Jeffery (1922) for comparison.

the matrix. The orientation of the shear bands in simple shear is similar in tapioca pearls with and without a central object (Figs. 10b and 12a). The shear bands are not stable in time. They either shift position in the matrix material or become inactive and are replaced by new bands that are initiated elsewhere. With a decreasing vorticity number the spacing between the shear bands increases and the shear bands develop at a larger distance from the object. The lower the vorticity number, the higher the angle of the shear bands with respect to the *xz*-plane of the apparatus (Fig. 12). The shear bands accommodate up to 60% of the strain in the experiments with a central object. The stable orientation of the objects in the simple shear experiments is with their long side approximately parallel to the shear bands. Some shear bands develop directly adjacent to the object in simple shear (Fig. 13), but this position is not stable. These shear bands also become inactive or shift through the material during progressive deformation. Fig. 12 shows the analyses of experiments with an object with $R_{ob} = 6$ in its stable position for different vorticity numbers. For the other objects the analyses look very similar for the same vorticity numbers. For the object with $R_{ob} = 6$ the long side is parallel to the shear bands for $W_k = 0.95$, but not for $W_k = 0.8$ and 0.6. For objects with $R_{ob} = 4$ and 10 in their stable positions the same is true. For an object with $R_{ob} = 3$ in its stable position, the long side is only parallel to the shear bands in simple shear, not in experiments with $W_k = 0.95$, 0.8 and 0.6.

5. Discussion

5.1. Discussion of experimental results

Results from experiments with monoclinic shaped objects in PDMS are very similar to the analytical solutions of Jeffery (1922) and Ghosh and Ramberg (1976) for the rotation of elliptical objects with the same aspect ratio in a Newtonian fluid. A monoclinic instead of an elliptical shape of the objects has little effect on the rotation behaviour of objects in PDMS both in simple shear (Arbaret et al., 2001) and for $W_k = 0.8$.

The experiments with tapioca pearls show completely different results. The square object ($R_{ob} = 1$) in simple shear is the only one that shows continuous clockwise rotation. In all other experiments with tapioca pearls the objects rotate towards a stable orientation, which has its long axis at a positive angle to the *x*-axis of the apparatus. The orientation depends on the aspect ratio of the object and the vorticity number. The reason for this difference in behaviour compared with the experiments with PDMS is the different deformation behaviour of the matrix material. In tapioca pearls a significant part of the deformation is concentrated in shear bands and the areas between the shear bands undergo only limited deformation. This localisation of the strain is more pronounced in experiments with a central object, where the shear bands accommodate 60% of the deformation. The objects are situated in the low

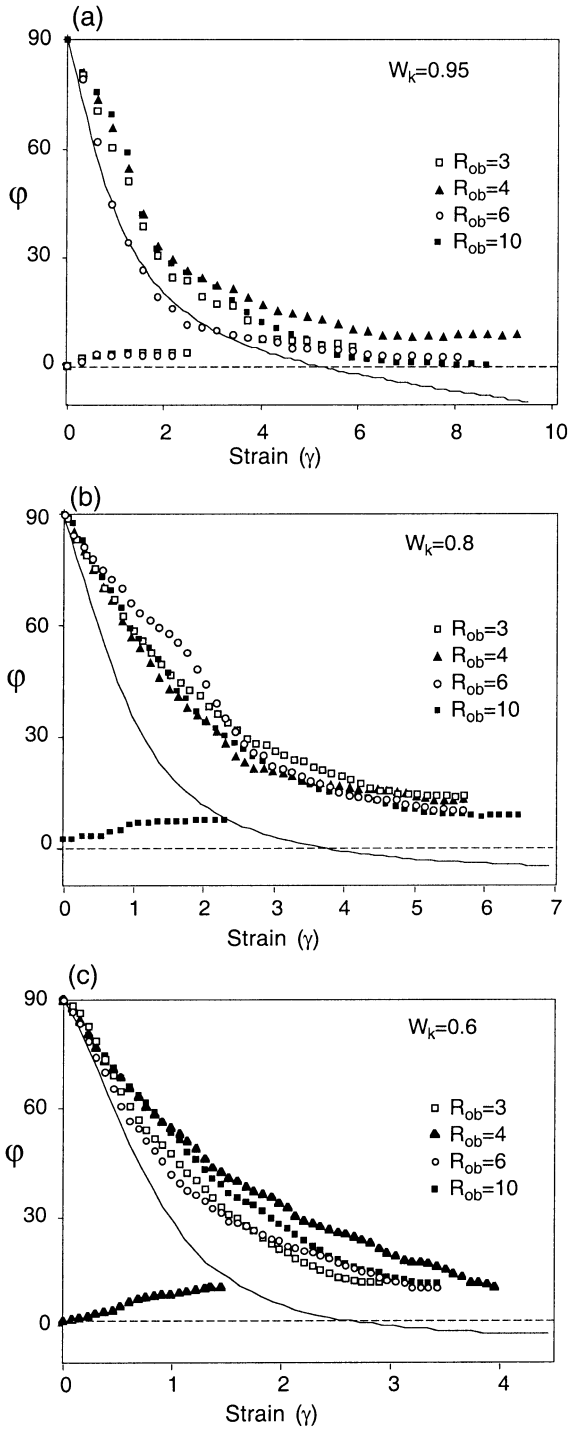

Fig. 8. Object orientation (φ) versus strain for experiments with tapioca pearls matrix at $W_k = 0.95$, 0.8, and 0.6. Initial orientation for the objects was $\varphi_0 = 90°$ for all combinations of W_k and R_{ob}, and $\varphi_0 = 0°$ for a few additional experiments. Solid lines are analytical solutions according to Jeffery (1922) for comparison.

deformation areas or microlithons and therefore rotate slower compared with rotation rates in analytical solutions and experiments with PDMS. The stable orientation of the monoclinic objects in the simple shear experiments and of the objects with $R_{ob} = 4$, 6 and 10 in experiments with

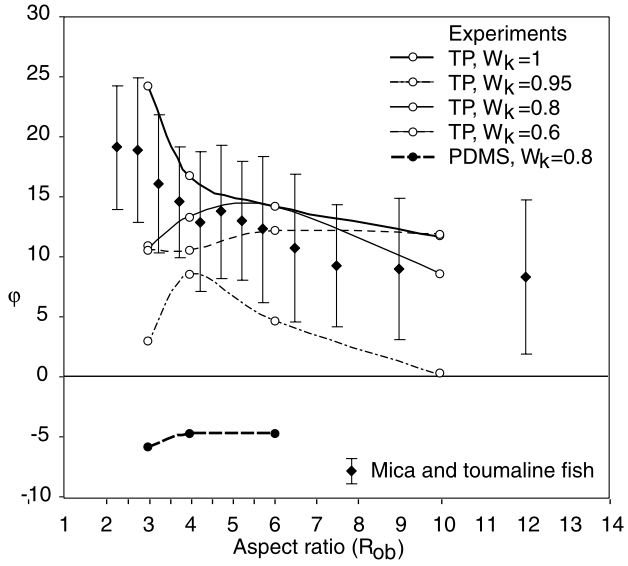

Fig. 9. Plot of stable object orientation (φ) versus aspect ratio (R_{ob}) for all performed experiments where a stable orientation was observed, together with the average values with standard deviations of the mica and tourmaline fish data.

$W_k = 0.95$ is with the long side of the object subparallel to the shear bands in the matrix (Fig. 12a and b). Therefore, in these experiments the orientation of the object is determined by the orientation of the shear bands, which is determined by the vorticity number. In the other cases, where the long side of the object is not parallel to the shear bands, the distance from the object to the closest shear bands is probably too large for the shear bands to have a direct influence on the orientation of the object. The orientation of the long axis of the objects seems to be independent of the aspect ratio of the object in the experiments with $W_k = 0.8$ and 0.6. The controlling factors for the orientation of the objects in these experiments is not clear, but is probably due to stress distribution in the complex arrangement of shear bands, matrix and object and due to the large component of pure shear flow in the deforming microlithon matrix. Incoherence of the matrix/object boundary (Ildefonse and Mancktelow, 1993; Pennacchioni et al., 2000) could also play a role in our experiments in attaining a stable orientation. Single particles with an incoherent object/matrix boundary in simple shear have slow rotation rates compared with objects with a coherent boundary in the experiments of Ildefonse and Mancktelow (1993) and a strong decrease in rotation rate was found for objects subparallel to the flow plane. These observations are similar to the results for objects in a tapioca pearl matrix. However, no concentration of strain was observed along the objects in our experiments.

5.2. Comparison of experimental results with measurements of mica and tourmaline fish

The measurements of natural mica and tourmaline fish

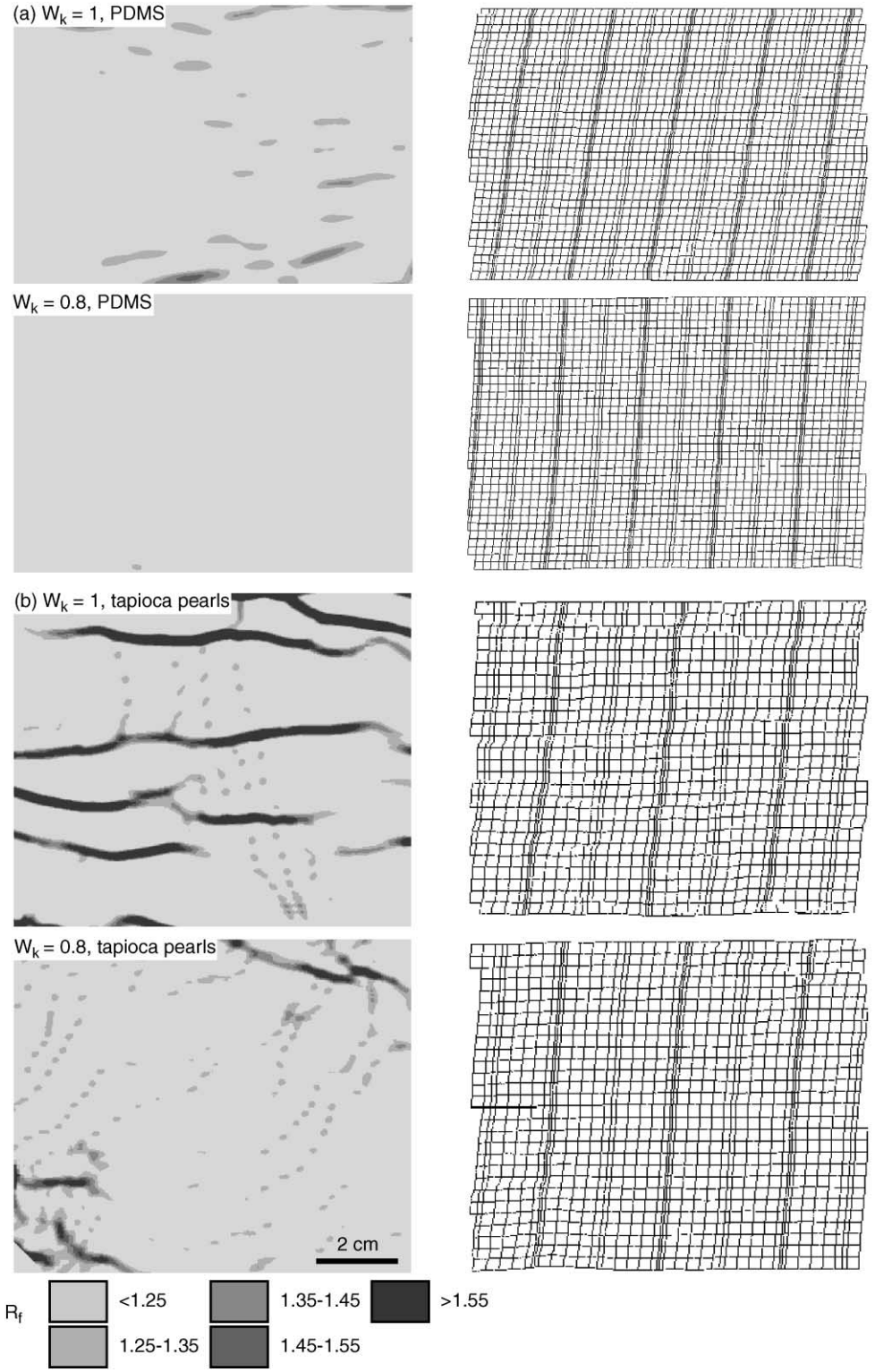

Fig. 10. Analysis of the distribution of strain in samples without rigid object, shown as grey scale plots of the finite strain ellipse axial ratio (R_f) and as deformed superimposed grids for strain increment of $R_f = 1.2$. (a) Deformation in PDMS is relatively homogeneously distributed throughout the sample and rarely exceeds the minimum finite strain value of $R_f = 1.25$ that can be resolved. (b) Deformation in tapioca pearls aggregates is localised in dextral shear bands represented by dark seams.

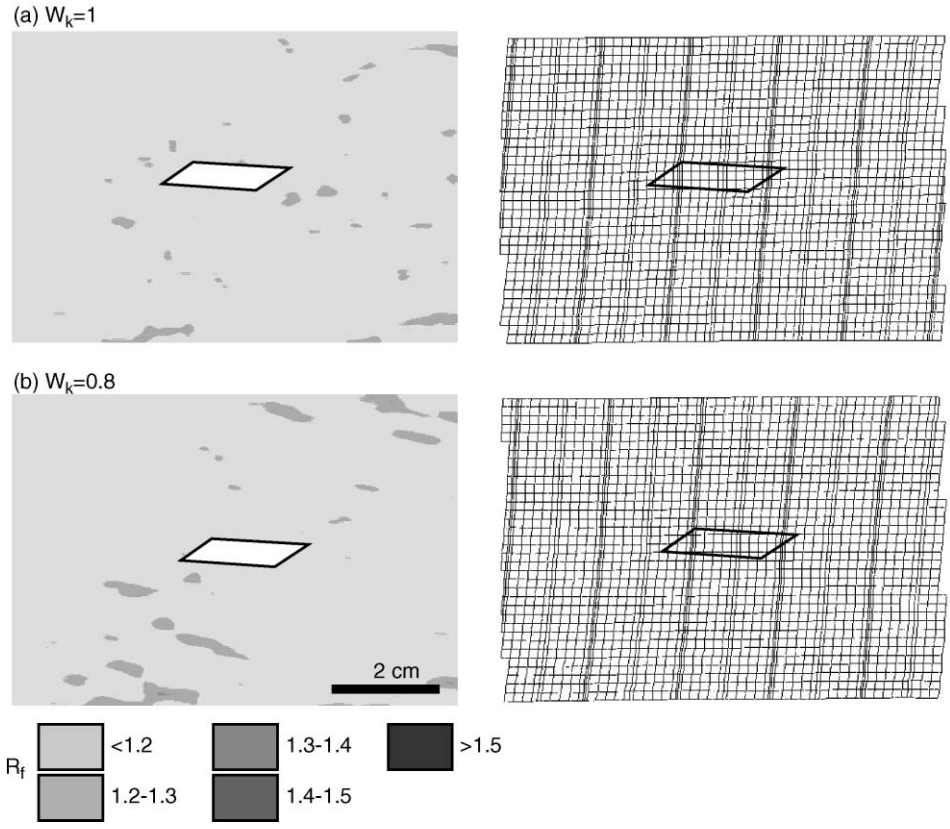

Fig. 11. Contours of R_f values and deformed grids for experiments with PDMS matrix and object with aspect ratio $R_{ob} = 6$. (a) Simple shear $W_k = 1$. (b) $W_k = 0.8$. Bulk strain is in both cases $R_f = 1.2$.

from three different shear zones show very similar results for each shear zone. On average the long axes of fish with a low aspect ratio have a slightly higher angle to the mylonitic foliation than the long axes of fish with a high aspect ratio (Fig. 9). To explain the orientation of the mineral fish in these measurements they are compared with the analytical solutions for rigid elliptical objects in Newtonian fluids (Jeffery, 1922; Ghosh and Ramberg, 1976) and to the experiments with monoclinic shaped objects in PDMS and tapioca pearls. For this comparison a few assumptions must be made. First of all the deformation of the mica and tourmaline fish should be minor relative to the deformation in the matrix in order to regard them as rigid objects. Although micas can be expected to deform internally by slip on the basal plane, it is striking that the geometry and orientation of mica fish is so similar to that of fish-shaped grains of tourmaline, kyanite and feldspars (Passchier and Trouw, 1996). They can also still be found as relatively large porphyroclasts in the intensely sheared matrix. This seems to indicate that, once the characteristic parallelogram or lenticular 'fish' geometry is established, mica grains deform very little internally. Secondly, there should be little interaction between the fish. The orientation of the fish is assumed to be only a function of their aspect ratio, and not influenced by interaction with neighbouring mineral fish. In our samples, the distance between the fish is usually large enough (more than a fish length) that interaction can be assumed to be negligible.

The trend of long axis orientation versus aspect ratio for the natural mica and tourmaline fish and the curves for analytical solutions for ellipses in a Newtonian fluid and experiments with PDMS as matrix material show very little resemblance (Figs. 2 and 9). A stable orientation (φ_{stable}) for the elongated objects can be found in experiments with a vorticity number $W_k < 1$, but the stable orientations as observed in these experiments and also the orientations resulting from analytical solution for elongated objects in viscous flow with $W_k < 1$ (Ghosh and Ramberg, 1976) all have negative angles, whereas the orientation of the natural mica and tourmaline fish usually has a positive angle. The orientation of the long object axis versus aspect ratio as observed for the natural mica and tourmaline fish is, however, similar to the stable orientations for rigid objects in a matrix of tapioca pearls, especially for simple shear deformation (Fig. 9).

Obviously, deformation mechanisms in the mylonite zones that contain mica and tourmaline fish are different from the mechanisms in our analogue materials. PDMS is a Newtonian viscous fluid; tapioca pearls a low cohesion granular material with Mohr–Coulomb type deformation. Nevertheless, it is remarkable that despite this difference such a close relation exists between mica fish in mylonites

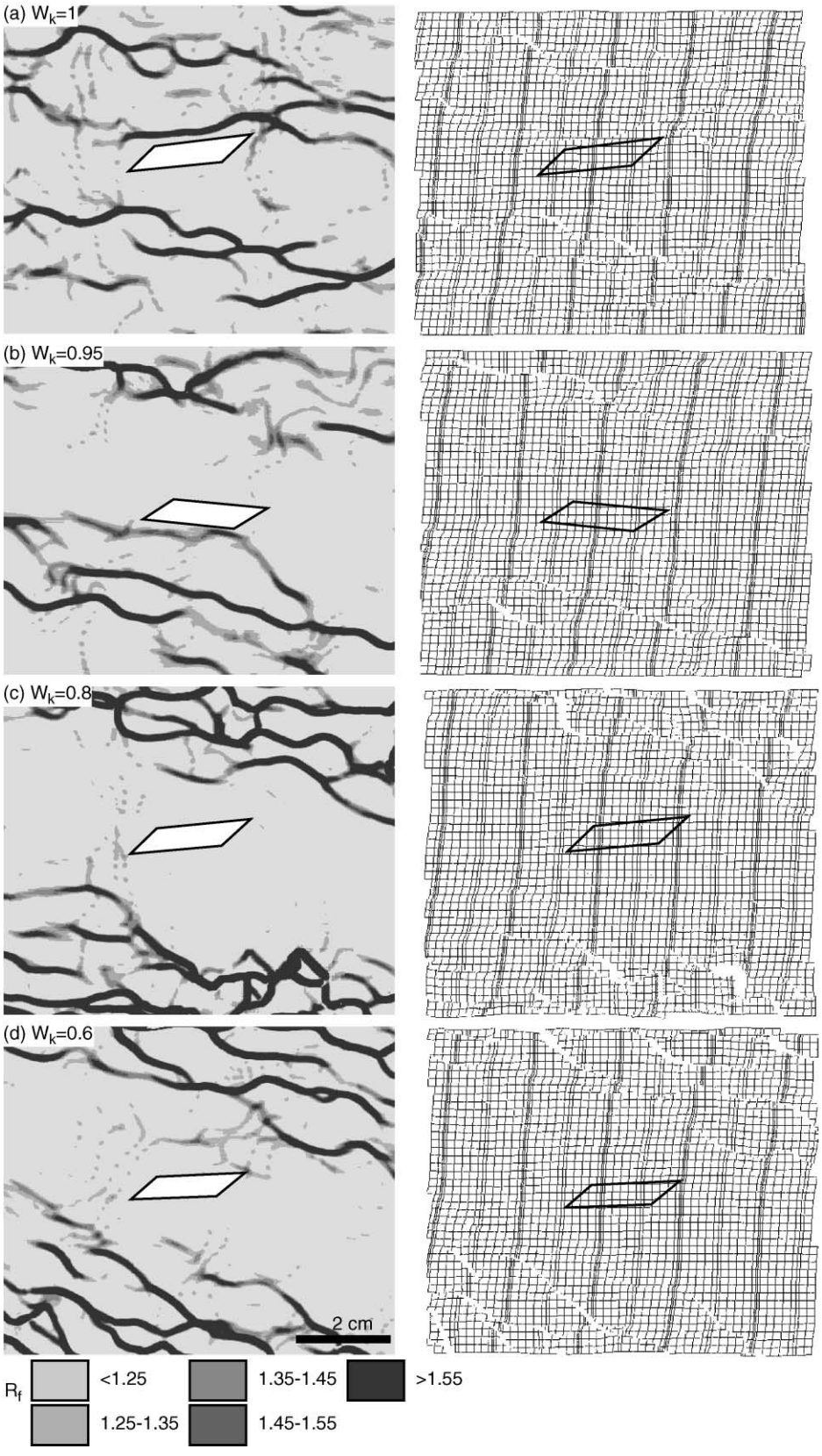

Fig. 12. Contours of R_f values and deformed grids for experiments with tapioca pearls matrix and object $R_{ob} = 6$. (a) Simple shear, $W_k = 1$, (b) $W_k = 0.95$, (c) $W_k = 0.8$, (d) $W_k = 0.6$. Dark bands are highest strain zones. Bulk strain is in all cases $R_f = 1.2$.

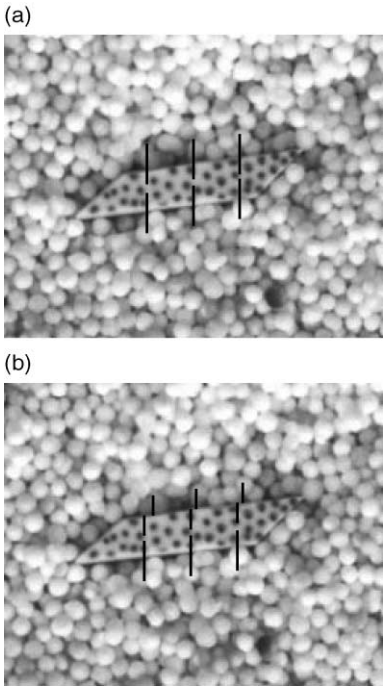

Fig. 13. Close-up of the area around the object for the experiment with tapioca pearls matrix and object $R_{ob} = 6$ and $W_k = 1$. Pictures (a) and (b), which were used to make Fig. 12a, are taken over a strain interval of $R_f = 1.2$. The offset of the three upper marker lines in (b) show that there is a shear band active along the upper boundary of the object during this interval, the other three straight marker lines show the absence of a shear band along the lower boundary of the object.

and rigid objects in tapioca pearls. This probably means that the crucial factor influencing the development of mica fish is flow kinematics. Deformation is localised in discrete small-scale shear bands in tapioca pearls. The similarity between the data from natural examples and results from experiments with a Mohr–Coulomb matrix suggests that there must be small-scale strain localisation in mylonites in order to form mica fish. Lister and Snoke (1984) predicted that mica fish are bordered by shear bands, but experiments with tapioca pearls suggest that shear bands can be further away and migrating through the sample with the same effect. Possibly, deformation in mylonites can be described by inhomogeneous flow that occurs by short living small-scale (<mm–cm) shear bands that shift position, as in tapioca pearls. Ongoing deformation and dynamic recrystallisation may overprint earlier fabrics and erase traces of flow partitioning (Bons and Jessell, 1999). This shifting and overprinting of shear bands may explain the absence of grain-size gradients or other signs of enhanced strain in a way that the sites of localisation cannot be determined from the microstructure at the end of the deformation history. This kind of small-scale flow partitioning, which is homogenised over time in progressive deformation has been observed in experiments with the polycrystalline material octachloropropane (Bons and Jessell, 1999). This type of behaviour may be responsible for the deformation in mylonites with mineral fish and a relatively homogeneous quartz matrix.

The observed decrease in angle with increasing aspect ratio of the mica and tourmaline fish of the natural samples fits best with the results of the simple shear experiments, where the orientation of the long side of the object is parallel to the shear bands. However, as mentioned in the previous section the distance of the shear bands to the objects is an important factor for the stable orientation of the objects in the experiments. In the experiments with $W_k < 1$, the distance between object and the nearest shear bands increases with decreasing vorticity number. Besides the vorticity, the distance from the object to the nearest shear bands probably also depends on the grain size of the experimental material. We did not test this effect of grain size, since in rocks the deformation mechanism is different. It is therefore not yet possible to draw any conclusions about the vorticity number in natural samples from the microstructure.

6. Conclusions

Analogue experiments on the rotational behaviour of elongated rigid objects were carried out using two end-member model materials: PDMS (Newtonian viscous polymer) and tapioca pearls (Mohr–Coulomb behaviour). Flow was modelled at several kinematic vorticity numbers. The results from the experiments with a PDMS matrix gave similar results as analytical solutions for ellipses in viscous flow (Jeffery, 1922; Ghosh and Ramberg, 1976), indicating that the aspect ratio, not the detailed shape is the controlling factor for the rotation behaviour of objects in viscous materials (Arbaret et al., 2001). The results of the experiments with a tapioca pearl matrix are completely different. Under all studied conditions, the elongated objects reach a stable orientation, between about $\varphi = 1$ and 25°. The deformation in tapioca pearls is concentrated in small shear bands on the scale of the pearls. Measurements of the long axis of natural samples of mica and tourmaline fish with respect to the mylonitic foliation show, on average, an inclined, positive φ-value. The average angle decreases with aspect ratio of the object. These data fit very well with the results from the experiments in tapioca pearls in simple shear, where the orientation of the object is determined by the orientation of shear bands. This indicates that strain localisation in micro-scale shear bands or zones is probably an important characteristic of the rheology of natural mylonites with mica fish or other 'mineral fish' and possibly of all mylonites. The presence of inclined fish-shaped objects may be indicative for micro-scale strain partitioning, even where no other microstructural indications for flow partitioning are found.

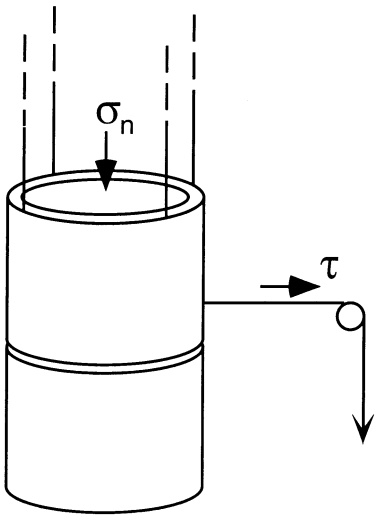

Fig. 14. Schematic drawing of the set-up used to measure the coefficient of internal friction and cohesion of tapioca pearls. Two cylinders are both filled with tapioca pearls. The bottom cylinder is fixed and the top cylinder is hanging on four cables, so the top cylinder can move frictionless with respect to the bottom one. The normal load is applied by the tapioca pearls in the upper cylinder and extra metal loads on top. The shear load is applied by the hanging mass over a pulley. Figure is not to scale.

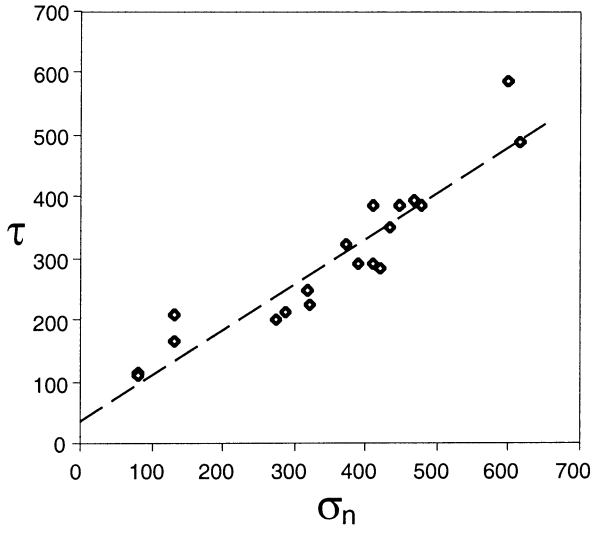

Fig. 15. Plot of data from shear test on tapioca pearls shown as shear stress versus normal stress. The line is the best fit by linear regression and indicates that for failure in this material $\mu = 0.74$ (slope) and $C_0 = 39$ Pa (intercept).

Acknowledgements

StG acknowledges financial support from the Deutsche Forschungs-gemeinschaft (GRK 392/1-99) and DAAD (415-br-probral). We are thankful for the thoughtful reviews provided by Rudolph Trouw and an anonymous reviewer.

Appendix A

Aggregates of tapioca pearls show Mohr–Coulomb type behaviour, where the shear stress (τ) for failure is related to the normal stress (σ_n) on the failure plane by:

$$\sigma_n = C_0 + \mu\tau$$

The coefficient of internal friction, μ, and cohesion, C_0, for tapioca pearls where determined using the method described by Krantz (1991). The simple apparatus consists of two compartments, the lower one fixed and the upper one supported by four cables of about 40 cm length (Fig. 14). The compartments are 7.5 cm high, have a cross-section of 4.35 cm and were both filled with the pearls. A horizontal fault is created in the pearls when the top cylinder is shifted. The overlying tapioca pearls and extra metal loads determine the normal load across the horizontal fault surface between the two cylinders. Tapioca pearls were poured to the desired depth above the fault plane and the extra load was put on top. A shear load was applied to the top cylinder by adding water to a container hanging over a frictionless pulley. The shear load was increased until a distinct failure event occurred. The data points of this experiment are plotted in Fig. 15 as normal stress (σ_n) versus shear stress (τ). The coefficient of internal friction, μ (slope) and cohesion, C_0 (intercept) follow from this plot. For tapioca pearls these values are $\mu = 0.74 \pm 0.05$ and $C_0 = 39 \pm 44$ Pa.

References

Arbaret, L., Diot, H., Bonchez, J.L., Saint Bdanquat, M., Lespinasse, P., 1997, Analogue 3D experiments of magnetic fabric developed in simple shear flow. In: Bochez, J.L. et al. (Eds.). Granites: from segregation of melt to emplacement fabric, 129–130.

Arbaret, L., Mancktelow, N.S., Burg, J.-P., 2001. Effect of shape and orientation on rigid particle rotation and matrix deformation in simple shear flow. Journal of Structural Geology 23, 113–125.

Azor, A., Ferando Simancas, J., Exposito, I., Gonzalez Lodeiro, F., Martinez Poyatos, D.J., 1997. Deformation of garnets in a low-grade shear zone. Journal of Structural Geology 19, 1137–1148.

Berthé, D., Choukroune, P., Jegouzo, P., 1979. Orthogneiss, mylonite and coaxial deformation of granites: the example of the South Armorican Shear Zone. Journal of Structural Geology 1, 31–42.

Bons, P.D., Jessell, M.W., 1995. Strain analysis in deformation experiments with pattern matching or a stereoscope. Journal of Structural Geology 17, 915–921.

Bons, P.D., Jessell, M.W., 1999. Micro-shear zones in experimentally deformed octachloropropane. Journal of Structural Geology 21, 323–334.

Bons, P.D., Barr, T.D., ten Brink, C.E., 1997. The development of ∂-clasts in non-linear viscous materials: a numerical approach. Tectonophysics 270, 29–41.

Eisbacher, G.H., 1970. Deformation mechanisms of mylonitic rocks and fractured granulites in Cobequid Mountains, Nova Scotia, Canada. Geological Society of America Bulletin 81, 2009–2020.

Ferguson, C.C., 1979. Rotations of elongated rigid particles in slow non-Newtonian flows. Tectonophysics 60, 247–262.

Fernandez, A., Feybesse, J.-L., Mezure, J.-F., 1983. Theoretical and

experimental study of fabrics developed by different shaped markers in two-dimensional simple shear. Bull. Soc. Geol. France 3, 319–326.

Freeman, B., 1985. The motion of rigid ellipsoidal particles in slow flows. Tectonophysics 113, 163–183.

Gay, N.C., 1968. Pure shear and simple shear deformation of inhomogeneous viscous fluids. 1. Theory. Tectonophysics 5, 211–234.

Ghosh, S.K., Ramberg, H., 1976. Reorientation of inclusions by combinations of pure and simple shear. Tectonophysics 34, 1–70.

Goodwin, L.B., Wenk, H.-R., 1995. Development of phyllonite from granodiorite: Mechanisms of grain-size reduction in the Santa Rosa mylonite zone, California. Journal of Structural Geology 17, 689–707.

Hanmer, S., Passchier, C.W., 1991. Shear sense indicators: a review. Geological Survey of Canada Paper 90, 1–71.

Hinch, E.J., Leal, L.G., 1979. Rotation of small non-axisymmetric particles in simple shear flow. Journal of Fluid Mechanics 92, 591–608.

Ildefonse, B., Mancktelow, N.S., 1993. Deformation around rigid particles: the influence of slip at the particle/matrix interface. Tectonophysics 221, 345–359.

Ildefonse, B., Launeau, P., Bouchez, J.-L., Fernandez, A., 1992a. Effect of mechanical interactions on the development of shape preferred orientations: a two-dimensional experimental approach. Journal of Structural Geology 14, 73–83.

Ildefonse, B., Sokoutis, D., Mancktelow, N.S., 1992b. Mechanical interactions between rigid particles in a deforming ductile matrix. Journal of Structural Geology 14, 1253–1266.

Jeffery, G.B., 1922. The motion of ellipsoidal particles immersed in a viscous fluid. Proceedings of the Royal Society of London, Series A 102, 161–179.

Jezek, J., Melka, R., Schulmann, K., Venera, Z., 1994. The behaviour of rigid triaxial ellipsoidal particles in viscous flows — modeling of fabric evolution in a multiparticle system. Tectonophysics 229, 165–180.

Kirby, S.H., Kronenberg, A.K., 1987. Rheology of the lithosphere: selected topics. Reviews of Geophysics 25, 1219–1244.

Krantz, R.W., 1991. Measurements of friction coefficients and cohesion for faulting and fault reactivation in laboratory models using sand and sand mixtures. Tectonophysics 188, 203–207.

Lister, G.S., Snoke, A.W., 1984. S-C mylonites. Journal of Structural Geology 6, 616–638.

Masuda, T., Michibayashi, K., Ohta, H., 1995. Shape preferred orientation of rigid particles in a viscous matrix: re-evaluation to determine kinematic parameters of ductile deformation. Journal of Structural Geology 17, 115–129.

Means, W.D., 1981. The concept of steady-state foliation. Tectonophysics 78, 179–199.

Means, W.D., Hobbs, B.E., Lister, G.S., Williams, P.F., 1980. Vorticity and non-coaxiality in progressive deformation. Journal of Structural Geology 2, 371–378.

Paciullo, F.V.P., Ribeiro, A., Andreis, R.R., 1993. Reconstrução de uma bacia fragmentada: o caso do Ciclo Depositional Andrelândia. In: Simp. Cráton do São Francisco, 2, Salvador, 1993, pp. 224–226.

Passchier, C.W., 1987. Stable positions of rigid objects in non-coaxial flow — a study in vorticity analysis. Journal of Structural Geology 16, 679–690.

Passchier, C.W., 1998. Monoclinic model shear zones. Journal of Structural Geology 20, 1121–1137.

Passchier, C.W., Simpson, C., 1986. Porphyroclast systems as kinematic indicators. Journal of Structural Geology 15, 895–910.

Passchier, C.W., Trouw, R.A.J., 1996. Microtectonics. Springer Verlag, Berlin, Heidelberg.

Pennacchioni, G., Fasolo, L., Morandi Cecchi, M., Salasnich, L., 2000. Finite-element modelling of simple shear flow around a circular rigid particle. Journal of Structural Geology 22, 683–692.

Piazolo, S., ten Grotenhuis, S.M., Passchier, C.W., 2001. A new apparatus for controlled general flow modeling of analog materials. In: Koyi, H.A., Mancktelow, N.S. (Eds.). Tectonic Modeling: A Volume in Honor of Hans Ramberg. Geological Society of America Memoir 193.

Ribeiro, A., Trouw, R.A.J., Andreis, R.R., Paciullo, F.V.P., Valença, J.G., 1995. Evolução das bacÍas Proterozóicas e o termo-tectonismo Brasiliano na margem sul do Cráton do São Francisco. Revista Brasileira de Geociências 25, 235–248.

Simpson, C., 1984. Borrego Springs–Santa Rosa mylonite zone: a late cretaceous west-directed thrust in Southern California. Geology 12, 1–11.

Simpson, C., Schmid, S.M., 1983. An evaluation of criteria to deduce the sense of movement in sheared rocks. Geological Society of America Bulletin 94, 1281–1288.

Simpson, C., De Paor, D.G., 1993. Strain and kinematic analysis in general shear zones. Journal of Structural Geology 15, 1–20.

ten Brink, C.E., 1996. Development of porphyroclast geometries during non-coaxial flow. Geologica Ultraiectina, 142 (Publ. PhD Thesis), Utrecht University, The Netherlands.

Tikoff, B., Teysier, C., 1994. Strain and fabric analyses based on porphyroclast interaction. Journal of Structural Geology 16, 477–491.

Trouw, R.A.J., Ribeiro, A., Paciullo, F.V., 1983. Geologia estrutural dos grupos São João del Rei, Carrancas e Andrelândia, Sul de Minas Gerais. An. Acad. brasil. Cienc. 55, 71–85.

Weijermars, R., 1986. Flow behaviour and physical chemistry of bouncing putties and related polymers in view of tectonic laboratory applications. Tectonophysics 124, 325–358.

Wenk, H.-R., Pannetier, J., 1990. Texture development in deformed granodiorites from the Santa Rosa mylonite zone, southern California. Journal of Structural Geology 12, 177–184.

White, S.H., Burrows, S.E., Carreras, J., Shaw, N.D., Humphreys, F.J., 1980. On mylonites in ductile shear zones. Journal of Structural Geology 2, 175–187.